Surface-emitting semiconductor laser spectroscopy for characterizing normal and sickled red blood cells*

P.L. Gourley, K. E. Meissner, T. M. Brennan, and B. E. Hammons

Sandia National Laboratories
Albuquerque, NM 87185

M. F. Gourley

National Institutes of Health
Bethesda, MD 20817

ABSTRACT

We have developed a new intracavity laser technique that uses a living or a fixed cell as an integral component of the laser. The cells are placed on an AlGaAs/GaAs surface-emitting semiconductor wafer and covered with a glass dielectric mirror to form a laser resonator. In this arrangement, the cells serve as optical waveguides (or lens elements) to confine (or focus) light generated in the resonator by the semiconductor. Because of the high transparency, the cells aid the lasing process to generate laser light. This ultra sensitive laser provides a novel imaging/spectroscopic technique for histologic examination which we demonstrate with normal and sickled human red blood cells. Extremely high contrast microscopic images of the cells are observed near 830-850 nm. These images correspond to electromagnetic modes of cell structures and are sensitive to shape of the cell. Using a high resolution spectrometer, we resolve the light emitted from these images into very narrow spectral peaks associated with the lasing modes. Analysis of the spectra reveals that the distribution of peaks is quite different for normal and sickled red blood cells. This technique, in a more developed form, may be useful for the rapid analysis of other kinds of normal and abnormal cells.

1. INTRODUCTION

In recent years the need for high speed analysis and micromanipulation of cells and cell components has been recognized. Semiconductor technology has many desirable attributes which can help to meet this need. Semiconductor structures and devices can be fabricated with nanometer to millimeter dimensions which span the range of sizes of cells and their components. These structures and devices can be readily manufactured at low cost to make them readily accessible to end users. Further, the manufacturing processes can integrate microsensors and analytical components on single chips for compactness.

Included in this technology are semiconductor microlasers and microoptics. New generations of semiconductor devices with lasing wavelengths that span useful ranges for cell diagnostics are being to appear in the commercial marketplace and in the research laboratory. Laser technology is well suited cell analysis because it is sensitive, very fast, and inherently compatible with parallel processing for high throughput. High resolution spectroscopy, ultrasensitive nonlinear optical processing, and probing on ultrashort time scales are possible. Laser probing can be non-invasive to probe cells in their physiologic state or used for microsurgery or for micromanipulation. Many of these capabilities can be integrated onto a semiconductor wafer.

The biomedical use of lasers in studying cells has expanded in recent years. Gas lasers are routinely used for sorting cell types[1] and characterizing cell physical properties.[2] Such lasers are also routinely used to study cell biochemistry by laser scanning confocal microscopy.[3] Further, lasers are used to micromanipulate cells and organelles by optical trapping.[4,5] Microsurgery at the cellular level can also be performed with short wavelength lasers.[6] All of these laser applications take advantage of specific light-cell interactions like light scattering, light induced fluorescence, refractance, or absorbance to extract cell information or modify the state of the cell. In all cases the cells are located outside the laser resonator and serve as passive scatters or absorbers.

Newly developing semiconductor lasers offer advantages over gas lasers in compactness, efficiency, and cost. They can be massively integrated or combined with other devices on a single wafer.[7] These features are highly desirable for biotechnologies which require miniaturization, parallelization (high throughput), and automation.[8]

2. OPTICS OF CELLS IN LASER CAVITIES

In this paper, we report new lasing phenomenon occurring in microcavities formed by placing normal and sickled human red blood cells inside a semiconductor laser cavity. The cavity comprises a dielectric mirror and a newly developed semiconductor laser wafer which emits in the near infrared where cells are highly transparent. The photon wavelength lies within the "therapeutic window" (transparent region from 700 to 1000 nm) so light is not absorbed by the cell to damage it. Thus, this biological microcavity laser, or "biocavity laser" for short, can non-invasively probe cells. Cell components with high refractive index act like optical waveguides to confine light and trigger laser action. The result is a lasing image of the cell. These images correspond to electromagnetic modes of cell structure and are sensitive to the size, shape, concavity of the red blood cells. Using a high resolution spectrometer, we resolve the light emitted from these images into very narrow spectral peaks associated with the lasing modes. We demonstrate that these peaks provide quantitative information about the cell structure. This is the primary focus of this paper. Beyond structural effects, we have evidence that this laser probe can be sensitive to minute changes in cell biochemistry. Subtle changes in DNA/protein structures in the cell will alter the local refractive index and change the lasing images and spectra. However, this topic is not discussed here.

2.1 General properties of red blood cells

Blood smears with normal and abnormal (sickled) cells are shown in Fig. 1. The normal red blood cell has a toroidal shape defined by an cytoskeletal network of spectrin.[9-11] In the normal red blood cell, the toroid diameter is about 7 μm and its thickness 2 μm. On an optical scale, the cell surface is smooth. The surface includes convex regions near the ring circumference and a concave region inside the ring. The former tend to concentrate light in the biocavity, the later diffuse it. With respect to the blood plasma, the hemoglobin/spectrin complex has a refractive index higher by about 2%.[12,13] Surprisingly, the refractive indices of hemoglobin and spectrin are almost perfectly matched.[13] The absorption coefficient of hemoglobin and water are less than 10^{-2} cm^{-1} near 850 nm where the biocavity lases.[14] Thus, red blood cells are nearly perfect optical elements (lenses) with little optical scatter (surface or internal) or optical loss. These cells are remarkably transparent near the light emission wavelengths 800-900 nm of commercially important semiconductors like gallium arsenide. Because of the high transparency, the cells aid the lasing process to generate laser light.

2.2 Waveguiding effects in a Fabry-Perot resonator

The help illustrate the waveguiding of light by cells, we have recorded ordinary near infrared transmittance micrographs of unstained red blood cells dried in air. A micrograph, shown in Fig. 2a, reveals that cells are highly transparent at these wavelengths. Also, the effects of light confinement can be seen. The image

shows a bright ring defined by the refractive index contrast between the red blood cell (high index) and surrounding air (low index). The same light focusing effects, though with less contrast, are present in cells in their hydrated physiologic state.

These micrographs suggest that light is focused by convex cell components with high refractive index as expected from the theory of geometrical optics. In a heterogeneous medium, the light rays bend toward the regions of higher refractive index.[15] For red blood cells the refractive index of hemoglobin is 1.40 compared to 1.35 for the blood plasma.[13] Thus, the entire hemoglobin-filled cell acts as a lens. The net effect of this focusing is to concentrate light to high index regions. The effect is evident with only a single pass of light through the cell as shown in Fig. 2a

This lateral confinement of light can be greatly amplified by placing the cells inside a Fabry-Perot resonator (two mirrors face-to-face) as illustrated in Fig. 2b. In the resonator, light undergoes multiple paths through the cell as it reflects from two external mirrors. Slight differences in refractive index between cell components and surrounding media produce an effective waveguide to confine light. Light rays (arrows) are shown for paths through convex surfaces of the red blood cell. These light rays tend to fold onto themselves to define stable optical modes. We have carried out a ray tracing analysis and have verified the existence of stable modes.[16] Light rays (leftmost arrows) are also shown passing through a concave surface of the red blood cell. These rays diverge and do not form stable optical modes.

2.3 Operation of the surface-emitting laser resonator

In the experiments described below, the mirrors of the Fabry-Perot resonator are two different types. The top is a dichroic multilayer dielectric on glass. The bottom mirror is a semiconductor multilayer grown epitaxially onto a gallium arsenide substrate.[7] Integrated onto this mirror is a semiconductor gain medium, shown in Fig. 2b, that provides photons and amplification for lasing in an optical mode supported by the cell. The gain/mirror combination takes the convenient form of a monolithic wafer that is compatible with standard microelectronic lithography. These surface-emitting laser wafers have been described in detail elsewhere.[7]

When the semiconductor gain region is photopumped by a separate pump laser,[17] electron-hole pairs are created in quantum wells. After a short delay of a few picoseconds, electrons and holes spontaneously recombine to emit light near 850 nm. If the pump beam is sufficiently intense, the pair density exceeds the transparency density near $1x10^{12}$ cm^{-3} and optical gain is developed. In this case, a spontaneously emitted photon can transit the cell, reflect from a mirror, and reenter the gain region. Here the photon can stimulate the recombination of another photon. The process is repeated till the light intensity is amplified many orders of magnitude on a time scale of picoseconds. Light passing through a cell has a higher probability of being amplified because of the waveguiding effect which helps concentrate the light. Some of the highly intensified light in the cavity leaks through the mirrors. The result is an intense, coherent light signal emitted from a region localized at the cell.

The semiconductor can be photopumped with several different laser sources. These sources include continuous wave, nanosecond, picosecond, and femtosecond pulsed lasers. The narrow pulse sources produce the highest electron-hole pair density and gain in the semiconductor. As the gain is increased in magnitude, it also increased in spectral width. The number of lasing modes described below will increase with the width of spectral gain.

Usually the laser is operated with a pump spot that is about 50 to 100 microns in diameter. This spot size is much larger than the cell diameter. If a cell is not present, only a weak, featureless, spontaneous emission spot from the pump area is observed. The measured spectrum exhibits a broad (several nanometers), weak peak. Dramatic changes occur when a cell is present. First very intense stimulated emission localized by the cell is observed. Second, the image appears as a distinct transverse electromagnetic mode of the resonator. Third, a very intense narrow spectral peak is observed in the spectrum. Finally, the emitted light is highly polarized compared to the spontaneous emission. All of these changes are characteristic of the lasing operation.

Photopumping the laser is not the most practical method of operating the surface-emitting laser. Ultimately, it is more desirable to electrically inject electrons and holes into the semiconductor via metal contacts. However, photopumping experiments provide a quick way of testing the concept without having to develop the complete device. Such experiments serve as a starting point to guide the development of such devices.

2.4 Analysis of the transverse optical modes in the laser resonator

For a biocavity shown in Fig. 2a, we model the cell as an object with refractive index n_1 (region 1) in a fluid of index n_2 (region 2) contained by two planar mirrors at positions -L/2 and L/2 along the z axis. Usually the cell will comprise proteins and DNA in the cytoplasm and will have an index somewhere near 1.4. The fluid is usually air, isotonic salt solution, or blood plasma. All of these have a lower index ranging from 1 to 1.35.

In the simplest analysis of optical modes in the biocavity, we are interested in solutions to the scalar wave equation

$$\nabla^2 E - \frac{n^2}{c^2}\frac{\partial^2 E}{\partial t^2} = 0 \qquad (1)$$

subject to a set of boundary conditions. We can separate the Laplacian operator into longitudinal and transverse parts and display the time dependence explicitly as,

$$(\nabla_\ell^2 + \nabla_t^2)E + \frac{n^2}{c^2}\omega^2 E = 0 \qquad (2)$$

The longitudinal operator can be replaced by $\nabla_\ell^2 \rightarrow -k_\ell^2$ where k_ℓ (also called β in the engineering literature) is the the longitudinal wavevector corresponding to the ℓth eigenmode of the Fabry-Perot cavity the solution of $\partial^2 E/\partial z^2 = -k_\ell^2 E$. The field amplitude will take the form $\cos(k_\ell z+\phi_m)$ or $\sin(k_\ell z+\phi_m)$ where ϕ_m is the sum of the mirror phases. The boundary conditions for the z dimension are that the field amplitude must be a null at $\pm L/2$. These conditions arise because the refractive index of the cell or fluid is lower than that of the bounding mirrors. The mirrors are multilayer dielectrics, but for simplicity we can treat them as hard edged metallic mirrors if we include a mirror phase. We anticipate that k_ℓ will be slightly smaller than the eigenwave vectors of a Fabry-Perot cavity filled uniformly with media of index n_1 but larger than that for index n_2.

The equation becomes

$$\nabla_t^2 E + \left(\frac{n^2\omega^2}{c^2} - k_\ell^2\right)E = 0 \qquad (3)$$

Since ω and k_ℓ are constants, the term in parenthesis will change as the refractive index changes between region 1 and region 2. In region 1 $\alpha^2 = n_1^2\omega^2/c^2 - k_\ell^2 > 0$ so the transverse solution will be oscillatory. In region 2, $\gamma^2 = n_2^2\omega^2/c^2 - k_\ell^2 < 0$ so the transverse solution will be evanescent.

At this point we have a qualitative picture of the eigenmodes, but we are interested in the eigenfrequencies. To compute these we need the exact solution for the transverse part of the field amplitude.

For simplicity, we can assume that the cell has cylindrical symmetry with diameter d. In this case Eqn 3 has normal and modified Bessel's functions $J(\alpha r)$ (oscillatory) and $K(\gamma r)$ (evanescent) for solutions inside and outside cell, respectively. The eigenfrequencies are found from

$$\alpha^2 + k_\ell^2 = \frac{n^2 \omega^2}{c^2} \tag{4}$$

The boundary conditions for dielectric discontinuities are that the transverse field components are continuous. However, very simple solutions can be found if the field amplitude vanishes at the boundary. This is a good approximation for the experimentally observed modes that are well contained by the cell. In this case, $\alpha \rightarrow \alpha_{mn} = 2x_{mn}/d$ where x_{mn} is the nth zero of the mth Bessel function. Since the field is contained within the cell $k_\ell = (2\pi\ell - \phi)n_1/2L$. The wavelengths of the eigenmodes are given by

$$\lambda_{\ell mn} = \frac{2\pi n_1}{\sqrt{\left[\frac{(2\pi\ell - \phi)n_1}{2L}\right]^2 + \left(\frac{2x_{mn}}{d}\right)^2}} \tag{5}$$

In practice, the field amplitude varies rapidly along z but very slowly along r so $k_\ell >> \alpha$. This is equivalent to saying that the lateral spectral modes are spaced much closer in frequency (and wavelength) than the longitudinal modes.

Under normal experimental conditions, the longitudinal modes are spaced more widely than the spectral gain. Thus, only one longitudinal mode will align with the gain spectrum to support lasing. Because of their smaller spacing, a large number of lateral modes will support lasing, depending on the magnitude of the gain and losses at these wavelengths. Further, two polarizations corresponding to transverse electric (TE) and transverse magnetic (TM) will be associated with each lateral mode.

We are interested in the spectrum of these lateral modes because it will be strongly influenced by the optical and structural properties of the cell. The separation of the lateral mode wavelengths from a given longitudinal wavelength will be given by

$$\Delta\lambda = \frac{-\lambda^3 x_{mn}^2}{2\pi^2 n_1^2 d^2} \tag{6}$$

A computed spectrum of lateral modes for a 7.5 μm diameter cell of refractive index 1.4 with light of wavelength 0.85 μm is schematically shown in Fig. 3. Each mode is represented by a vertical line positioned on a wavelength axis. Above the line, the modes indices mn are given. Also shown are experimentally observed lasing images corresponding to the six lowest order modes in normal red blood cells.

3. NORMAL RED BLOOD CELLS

3.1 Lasing modes of cells under low gain conditions

Lasing images of freshly drawn, normal red cells in whole blood diluted with isotonic salt solution are shown superposed on the computed spectral lines in Fig. 3. These images demonstrate that the cells support transverse electromagnetic (TEM) modes similar to those observed in other cylindrical laser resonators described in textbooks.[16] Each image corresponds to a single transverse eigenmode of the laser resonator. These images are recorded with either a cw or nanosecond pulsed pump laser. With these pump sources, the spectral gain is minimal and only one transverse mode is typically observed.

The frequency of occurrence of a given mode depends on the distribution of cell size and shape. The most frequently occurring mode is the TEM_{10} mode. The subscripts mn denote the number of angular and radial nodes (dark areas), respectively. This double-lobed mode is characteristic of about 50 percent of normal red blood cells in plasma in the physiologic state. Another common mode (not shown in Fig. 3) occurring in about 10 percent of the cells, is observed as a ring. This is the transverse electromagnetic mode designated TEM_{10}*. The star superscript denotes a linear combination of horizontal and vertical versions of TEM_{10} mode. Both of these modes exhibit nodes (dark areas) near the cell center and are consistent with the toroidal shape of the cells observed under brightfield microscopy (see the light rays in Fig. 2b). The fundamental TEM_{00} modes occurs in about 15% of the cells. These are probably associated with spherocytes or cells that have lost some of their biconcavity. The higher order modes TEM_{20} (cloverleaf), TEM_{30} (hexagonal), TEM_{01} (dot and ring, and TEM_{02} (split dot and ring) are observed much less frequently (each accounting for a few percent of the distribution). These modes occur in the largest cells where higher orders modes are stable.

3.2 Lasing modes under high gain conditions

The laser can also be operated with femtosecond pumping. In this case the spectral gain is very broad and many transverse modes can simultaneously support lasing. The observed distribution of spectral intensities of the modes will depend on the relative gain and loss for each mode. The relative loss will be determined by the geometry and optical diffraction of the cell. Also, the spectral separation of the modes will decrease with cell diameter. We hypothesize that each cell will have a unique spectral distribution of transverse modes. As a consequence we will have a precise way of to caliper the cell and its shape on ultrashort time scale.

3.2a Images and spectra

Images (insets) and spectra of three normal red blood cells used with femtosecond pumping are shown in Fig. 4. The three cells correspond to different diameters ranging from 5 to 7.5 μm. In each case, the image and spectrum comprise many different transverse modes operating simultaneously. The spectra are displayed on a log scale (spanning 3 orders of magnitude from background to highest peak) to enhance weaker modes. No absolute wavelength scale is given because the cells were examined at different positions in the Fabry-Perot cavity corresponding to slightly different mirror spacings and longitudinal mode wavelengths. Only the relative spectral positions of the modes are correlated with the cell properties. The spectra were recorded with the longest wavelength observed lasing mode positioned rightmost in the spectrum.

In Fig. 4, the 5.0 μm cell spectrum in the lower photo exhibits a dominant TEM_{00} mode and a less intense TEM_{10} mode. Consistent with this distribution, the inset image appears as a Gaussian disk. This smaller spherocyte has little biconcavity and favors the fundamental mode. Note the wide 5.5 nm spectral separation of the peaks in this spectrum due to the small cell size. The 5.7 μm spectrum in the center photo exhibits a dominant TEM_{10} mode, a less intense TEM_{00} mode, and a very weak TEM_{20} mode. The dominant mode is

evident in the double-lobed image. This cell has more biconcavity to favor the first overtone. Note the smaller 4.6 nm separation of the peaks.

The uppermost photo shows an image and spectrum of a larger 7.5 μm cell. The spectrum reveals 7 operating modes. The dominant mode is TEM_{10} and is identified by the lasing image near threshold (not shown). The higher order modes decrease almost monotonically to shorter wavelength. The separation of these modes is small (typically 1 to 2 nm) due the larger cell size. The spacings of the lowest order modes are in general agreement with computed line spacings in Fig. 3. Note in particular the close spacing of the TEM_{20} and TEM_{01} modes (2 large peaks nearest the dominant peak). The spacings of the three highest order modes are much less than those predicted in Fig. 3. This is expected since the optical field intensity for these modes leaks outside the cell boundaries contrary to perfect optical confinement in the model.

3.2b Cell size effects on the lasing spectra

Many images and spectra like those in Fig. 4 were recorded for cells of varying sizes. Using these data we were able to investigate the dependence of the spectral peak separation as a function of the cell diameter. The cell diameters in normal blood smears were in the range 6.5 to 8.5 μm. This relatively narrow distribution in diameters is evident in the normal blood smear of Fig. 1. Most of the cells in this micrograph have similar shapes and degree of biconcavity. Smaller diameter normal cells were obtained from the sickled blood smear. These smaller cells ranged from 5 to 6 μm in diameter and were more spherical.

In Fig. 5 the spectral separation of the TEM_{00} and TEM_{10} peaks is plotted against the cell diameter measured visually through a microscope. The separation decreases from about 1nm for the largest cells to near 5 nm for the smallest cells. The power dependence of $d \sim \lambda^n$ where n is between 2 and 3. A least squares fit of these data yields a power exponent of 2.8. This is higher than expected from Eqn. 6 which predicts a power exponent of 2. The discrepency may arise from using cells from 2 different blood samples. Despite this discrepancy, the strong dependence of the mode separation on cell size is demonstrated by these data.

In addition to red blood cells, white blood cells and platelets were observed to support lasing modes. The modes of the nucleated white blood cells are much more complex than red blood cells and will not be discussed here. The blood platelets are very small disks 1 to 4 micrometers in diameter. During lasing, the entire disk appears bright, suggesting operation in a TEM_{00} mode. The lasing spectra reveal one or two lasing modes. In Fig. 5, the spectral separation two lasing modes for a platelet is plotted. The data point is clearly away from the locus of points formed with the red blood cell data. This difference suggests that the refractive index of the platelet differs from that of the red blood cells.

4. SICKLED RED BLOOD CELLS

We also tested the biocavity laser for its sensitivity to abnormal blood cells. We selected sickled red blood cells since they correspond to one of the best understood molecular diseases.[9] In this disease, the hemoglobin molecule (HbS) has one amino acid substitution in the globulin chain whi ch causes the HbS protein to partially crystallize within the cell. With solid and liquid phases present, the cell acquires the characteristic shape of a sickle. Whole blood from a patient with sickle cell anemia (HbSS) was drawn and diluted in isotonic media and tested in the biocavity under high gain conditions like the normal red blood cells displayed in Fig. 4.

4.1 Theoretical spectrum

A theoretical spectrum was computed and is displayed in Fig. 6. In this calculation, the sickled cell is assumed to take a long, thin shape in contrast to the circular cell analysis of section 2.4. Eqns 1-3 of that analysis are valid, but Eqns 4-6 must be modified for this geometry. In Eqn 4 we replace ^{2} with $k_s^2+k_S^2$ with terms for the short and long axes of the sickled cell. The resulting transverse modes computed by this method

more than the number of nodes) along the short and long axes, respectively.

4.2 Images and Spectra

The experimental images and spectra for three sickled cells of different length are shown in Fig. 7. All of the lasing images reveal the linear geometry of the sickled cells which have long and short axes. Each image exhibits nodes along the length of the sickled cells. These images resemble the lower set of images drawn in the theoretical spectrum of Fig. 6. The number of nodes increases from 2 for the 8.2 μm cell to 3 for the 9.0 μm cell to 7 for the 11.6 μm cell. The images suggest that the lowest order modes (TEM_{11} or TEM_{21} with 1 or 0 nodes) are not present. The spectra in fig. 7 confirm this suggestion. All of the images have 2 or more nodes.

In the lower spectrum for the 8.2 μm cell, the longest wavelength peaks on the right side are broad and weak. These peaks correspond to the TEM_{11} and TEM_{21} modes and do not support lasing. The dominant peak TEM_{31}, third from the right, corresponds to the observed image with 2 nodes. Two other lasing peaks occur at shorter wavelength. The peaks are widely and equally separated by about 2 nm.

The central spectrum for the large 9.0 μm cell comprises 3 broad, weak peaks at long wavelength and 3 strong peaks at shorter wavelength. These peaks correspond to the TEM_{11}, TEM_{21}, and TEM_{31} modes which are not supporting lasing or marginally supporting lasing. The dominant peak is the TEM_{41} mode, fourth from the right, and corresponds to the image with 3 nodes. The peaks are more closely but equally spaced by about 1.7 nm.

In the uppermost spectrum for the 11.6 μm cell, many closely spaced peaks are evident. This spectrum is more complicated than the previous two. The peaks are not uniformly spaced and the distribution of lasing modes is less well defined. One peak at the extreme left dominants the spectrum. The postion in the spectrum identifies it as the TEM_{71} mode. This mode has 6 nodes and is consistent with the image superposed on this spectrum. Two weaker lasing modes are evident in the central part of the spectrum. The other broad peaks are modes that do not support lasing.

4.3 Comparison of results for sickled and normal cells

The images and spectra are quite different from those for normal red blood cells. In normal cells the fundamental and first overtone supported lasing. In the sickled cells only the second or higher overtones supported lasing. This is consistent with the linear structure of the sickled cell. The bright antinodes in images are almost always bright spots. The horizontal and vertical dimensions of these spots do not vary by more than a factor of 2 or so. Linear spots are not observed because of the anisotropy in optical diffraction in the two dimensions. Thus, long objects tend to break up into segmented antinodes.

We also found that the pump power for lasing threshold was higher by 50% than that for normal cells. This is probably a consequence of the larger dimension of the sickled cell. A circular pump spot is more effective in pumping a circular cell area. Another explanation is that the sickled cells are expected to be optically turbid entities that absorb or scatter light to lower the quality of the lasing resonance. Light scattering is expected from phase boundaries of the crystalline/liquid hemoglobin in the sickled cell. Increased absorption may be due to the crystalline phase of hemoglobin.

5. SUMMARY

We have examined the lasing modes and spectra of blood cells configured as a biological microcavity laser. Operation of this laser provides high contrast, coherent light images which are localized in the cell. The images

5. SUMMARY

We have examined the lasing modes and spectra of blood cells configured as a biological microcavity laser. Operation of this laser provides high contrast, coherent light images which are localized in the cell. The images correspond to lasing modes which are defined by the contrast in the refractive index of the cell relative to its surrounding fluid. Corresponding to this images are lasing spectra with very sharp lines sensitive to slight changes in the cell diameter and shape. We found that operation of the laser under low gain conditions produced simple spectra corresponding to only one lasing mode. Under high gain conditions, many lasing modes operated simultaneously. The spectrum of modes was different for normal and sickled cells. The lowest order modes were preferred in normal circular cells while higher order modes were preferred by the linear structure of the sickled cell.

6. ACKNOWLEDGEMENTS

We thank A. E. McDonald for assistance in obtaining the images and spectra.
*This work was sponsored by the United States Department of Energy under contract number DE-AC0494AL85000, and supported in part by the Division of Materials Science, Office of Basic Energy Science.

7. REFERENCES

1. see for example, *Flow cytometry and Sorting,* 2nd Ed., Edited by M. R. Melamed, Wiley-Liss (New York, 1990).
2. R. Bayer and G. Wolf, *Society of Photo-Optical Instrumentation Engineers,* **1981**, 26 (1992).
3. see for example, *Methods in Cell Biology, vol. 38, Cell Biological Applications of Confocal Microscopy,* edited by B. Matsumoto, Academic Press (San Diego, 1993).
4. S. M. Block, in *Noninvasive Techniques in Cell Biology,* Chap. 15, Wiley-Liss (New York, 1990).
5. A. Ashkin and J. M. Dziedzic, *Science* **235**, 1517 (1987).
6. R. Wiegand-Steubing, S. Cheng, W. H. Wright, Y. Numajiri, and M. W. Berns, *Cytometry* **12,** 505 (1991).
7. P. L. Gourley, *Nature,* October 13, 1994. P. L. Gourley, K. L. Lear, and R. P. Schneider, *IEEE Spectrum*, p 31-37, August, 1994.
8. These features are crucial to the development of advanced technologies for high speed DNA diagnostics, for example.
9. J. E. Darnell, H. F. Lodish, and D. Baltimore, in *Molecular Cell Biology,* 2nd Ed., Scientific American Books, W. H. Freeman and Co. (New York, 1990).
10. L. Weiss, in *Histology,* 5th Ed., Elsevier Biomedical, (New York, 1983), chap. 11.
11. L. Stryer, *Biochemistry,* 3rd Ed., W. H. Freeman and Co. (New York, 1988), chap 12.
12. We have estimated the refractive index difference between red blood cells and blood plasma using Nomarski phase contrast microscopy of freshly drawn whole blood. see also R. Barer, *J. Opt. Soc. Am.* **47,** 545 (1957).
13. M. Andersen and S. Nir, *Polymer* **18,** 867 (1977).
14. V. V. Tuchin, *Society of Photo-Optical Instrumentation Engineers,* **1981**, 2 (1992).
15. M. Born and E. Wolf, in *Principles of Optics,* 6th ed., Pergamon (New York), 1980, chap. 3.
16. see A. Yariv, in *Optical Electronics,* 3rd ed., Holt, Rinehart, and Winston (New York, 1985), chaps. 2 and 4.
17. The semiconductor is pumped through a microscope by a separate laser operating from 700 to 800 nm (alternately, it could be electrically injected). Using a CCD camera, the images are recorded in real time with

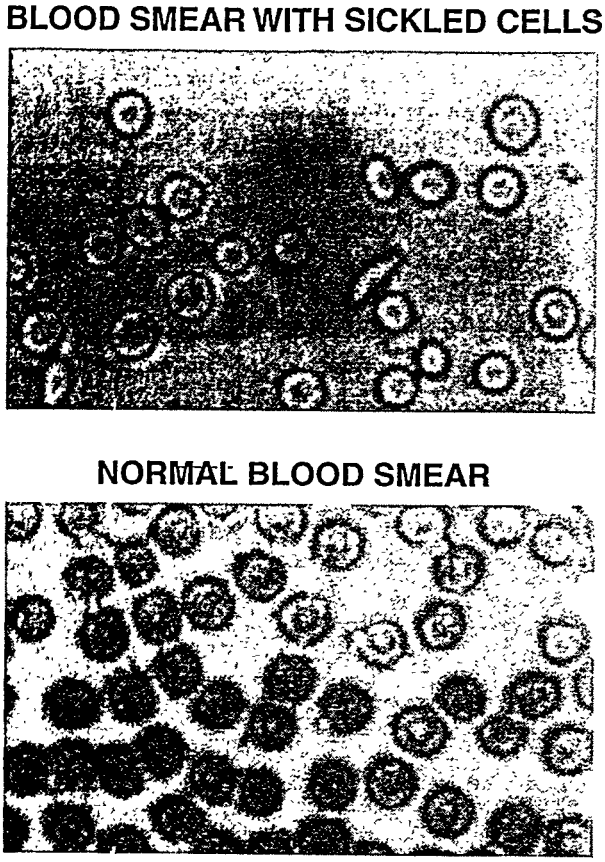

Fig. 1. Optical micrographs of blood smears with normal (lower photo) and sickled (upper photo) red blood cells.

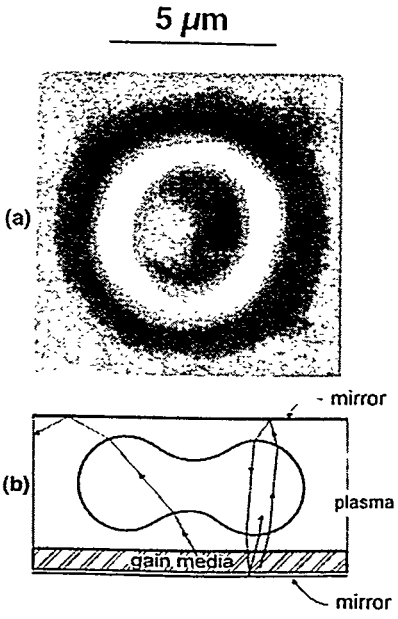

Fig. 2. (a) Optical micrograph of a red blood cell recorded in transmittance with near infrared light. The cells are part of an unstained blood smear dried in air. (b) Schematic cross sections of a red blood cell placed in a Fabry-Perot resonator (two facing mirrors) with a semiconductor gain medium. The arrows show possible optical pathways in the resonator corresponding to stable (folded paths) and unstable (unfolded) optical modes.

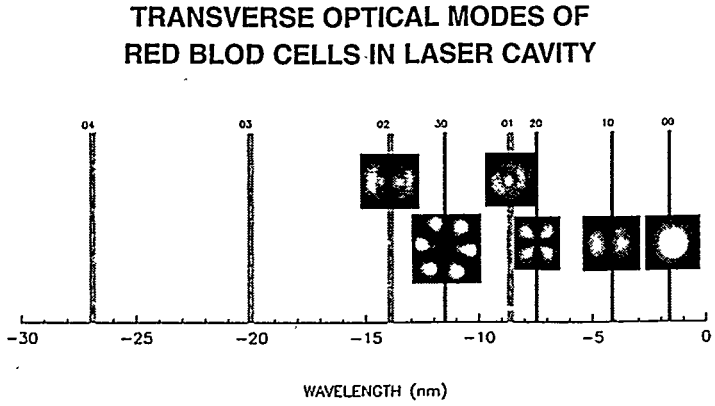

Fig. 3. Computed spectral lines for transverse optical modes for a cylindrical waveguide (approximating a red blood cell) in a Fabry-Perot resonator. The spectral lines are labled by indices mn, the order and zero of Bessel functions. Experimental near field micrographs of lasing modes supported by normal red blood cells are shown over the corresponding spectral lines.

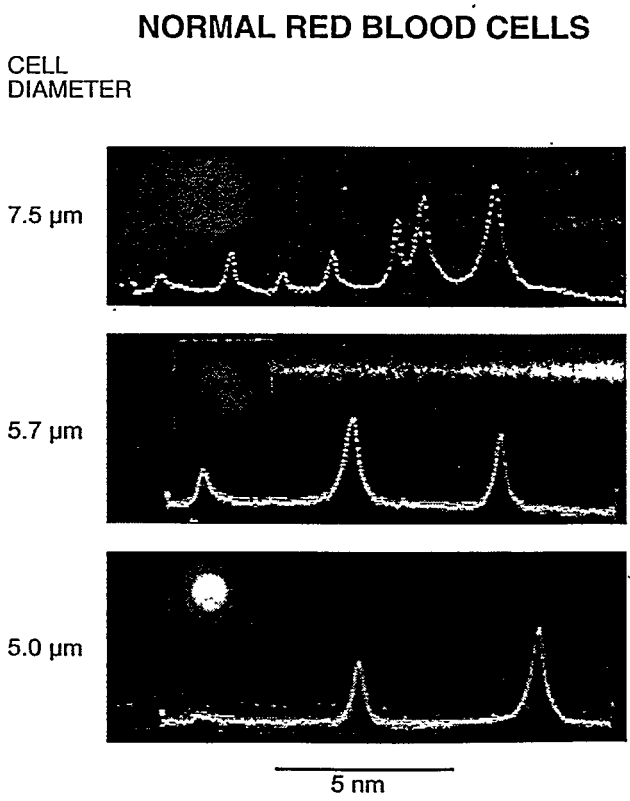

Fig. 4. Near field lasing micrographs and spectra of three different sized normal red blood cells from freshly drawn whole blood placed in a Fabry-Perot resonator.

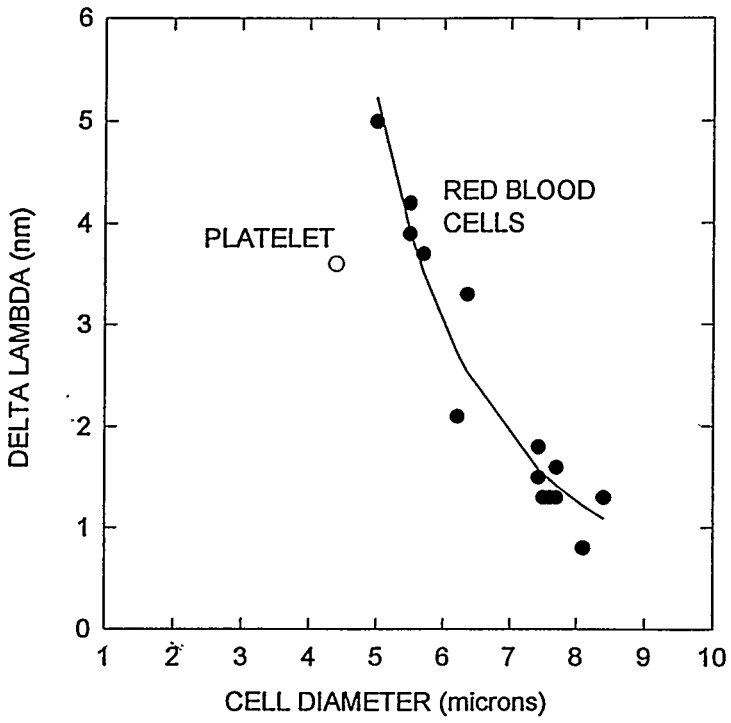

Fig. 5. Experimental spectral separation $\Delta\lambda$ between the fundamental (m=0, n=0) and first overtone (m=1, n=0) as a function of measured cell diameter for normal red blood cells. For comparison the result for a blood platelet are also shown.

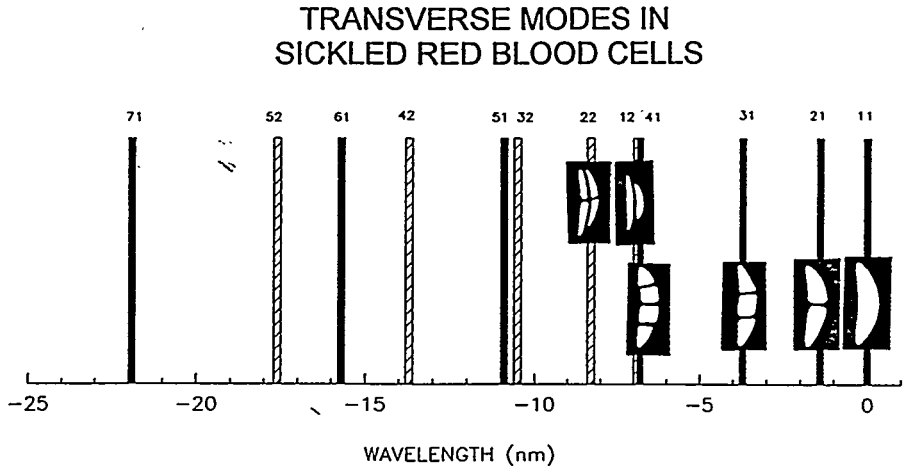

Fig. 6. Computed spectral lines and schematic images for transverse modes for sickled red blood cells.

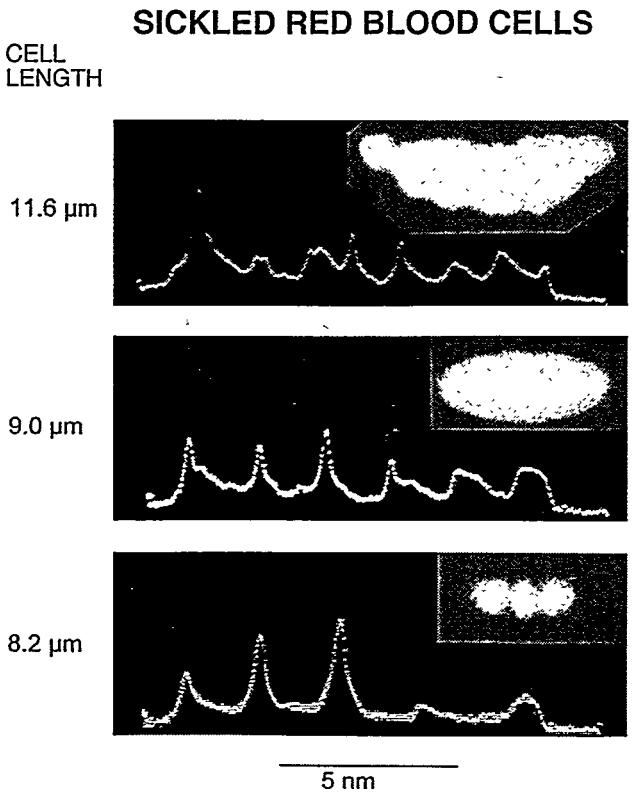

Fig. 7. Near field lasing micrographs and spectra of three different sickled red blood cells from whole blood placed in the Fabry-Perot resonator.

DISCLAIMER